

Article

Spatiotemporal Analysis of Future Precipitation Changes in the Huaihe River Basin Based on the NEX-GDDP-CMIP6 Dataset and Monitoring Data

Min Tong¹, Leilei Li^{1,*}, Zhi Li^{2,3}  and Zhihui Tian¹

¹ School of Earth Science and Technology, Zhengzhou University, Zhengzhou 450000, China; tongmin@gs.zzu.edu.cn (M.T.); iezhtian@zzu.edu.cn (Z.T.)

² China Center for Resources Satellite Data and Application, Beijing 100094, China; lizhi@lreis.ac.cn

³ China Siwei Surveying and Mapping Technology Co., Ltd., Beijing 100086, China

* Correspondence: stonejdx@zzu.edu.cn; Tel.: +86-189-1171-9037

Abstract: This research analyzes extreme precipitation events in the Huaihe River Basin in China, a densely populated region with a history of human settlements and agricultural activities. This study aims to explore the impact of extreme precipitation index changes and provide decision-making suggestions for flood early warning and agricultural development in the Huaihe River Basin. The study utilizes the NEX-GDDP-CMIP6 climate model dataset and daily value dataset (V3.0) from China's national surface weather stations to investigate temporal and spatial changes in the extreme precipitation indices from 1960 to 2014 and future projections. At the same time, this study adopts the RclimDex model, Taylor diagram, and Sen+Mann–Kendall trend analysis research methods to analyze the data. The results reveal a slight increase in extreme precipitation indices from the northwest to southeast within the basin, except for the CDD, which shows a decreasing trend. Regarding the spatial variation, the future increase in extreme precipitation in the Huaihe River Basin shows a spatial variation characteristic that decreases from the northwest to southeast. These findings suggest that extreme precipitation events are intensifying in the region. Understanding these trends and their implications is vital for adaptation strategy planning and mitigating the risks associated with extreme precipitation events in the Huaihe River Basin.

Keywords: NEX-GDDP-CMIP6; extreme precipitation; climate change; Huaihe River Basin



Citation: Tong, M.; Li, L.; Li, Z.; Tian, Z. Spatiotemporal Analysis of Future Precipitation Changes in the Huaihe River Basin Based on the NEX-GDDP-CMIP6 Dataset and Monitoring Data. *Water* **2023**, *15*, 3805. <https://doi.org/10.3390/w15213805>

Academic Editors: João Filipe Santos and Pavel Groisman

Received: 9 September 2023

Revised: 25 October 2023

Accepted: 26 October 2023

Published: 31 October 2023



Copyright: © 2023 by the authors. Licensee MDPI, Basel, Switzerland. This article is an open access article distributed under the terms and conditions of the Creative Commons Attribution (CC BY) license (<https://creativecommons.org/licenses/by/4.0/>).

1. Introduction

In the past 100 years, the global climate has experienced changes characterized by warming. Extreme weather and climate events are more likely to occur on a global and regional scale, which have substantially negatively impacted ecosystems [1]. The Green Paper on Climate Change highlights that China is one of the regions notably influenced by climate change. Since the mid-20th century, the rate of temperature increase has exhibited a markedly elevated trajectory compared to the global average for the corresponding temporal span [2]. The harmful consequences of climate change in China predominantly outweigh any potential benefits [3]. Therefore, studying the potential changes in the extreme precipitation index due to future climate change is of great scientific significance for implementing corresponding mitigation and adaptation measures in the study area.

Severe precipitation events substantially influence human safety, socio-economic advancement, and the integrity of natural ecosystems [4,5]. The frequency and intensity of extreme precipitation events in China and worldwide are increasing with global warming [6,7]. The IPCC Sixth Assessment Report points out that for every 1 °C increase in the global temperature in the future, the intensity of extreme daily precipitation events will increase by 7% [8]. Specifically, the research published by Shahi [9,10] in 2021 and 2023 provide in-depth analyses of the projected changes in the mean and intra-seasonal

variability of the Indian summer monsoon, as well as the future changes in high-impact precipitation events for India. Such findings underline the importance of understanding and preparing for these shifts, especially in regions that are particularly vulnerable to changes in monsoonal patterns and extreme precipitation events. Furthermore, the power of regional extreme precipitation has a nearly linear relationship with the extent of global warming. The greater the degree of global warming in the future, the more significant the increase in heavy precipitation. The Huaihe River Basin is prone to intense and continuous rainfall events, which lead to severe flood disasters. The accurate identification of temporal and spatial variation characteristics has become the focus of global attention [11].

Historically, the Huaihe River Basin has experienced frequent and severe extreme climate events. According to the statistics, there were 979 floods in the Huaihe River Basin between 246 BC and 1948. Particularly during the 754 years following the Yellow River's capture of the Huaihe River (1194–1948), the region witnessed a staggering 594 significant flood events, translating to an average of 79 catastrophic inundations every century [12]. The years of 1954, 1991, and 2003 were the three periods with abnormal precipitation levels in the Huaihe River Basin since the founding of the People's Republic of China [13]. In the summer of 2007, the Huaihe River Basin faced historically unprecedented flood disasters, with many major cities and regions enduring sporadic torrential downpours, leading to a complex disaster scenario [14]. Since early July 2021, Henan Province has faced severe disasters that are rare in history. Especially, on 20 July, Zhengzhou city suffered heavy rain and severe floods that caused heavy casualties and property losses. Hence, policymakers and the general populace must comprehend extreme precipitation's temporal and spatial evolutionary traits within the Huaihe River Basin. A sophisticated analysis of the long-term extreme precipitation index proves instrumental in enhancing disaster prevention and mitigation strategies.

At present, climate models are widely used for extreme precipitation simulations and future predictions. The new round of the International Coupled Model Intercomparison Project (CMIP6) released the output results of atmospheric circulation models developed by more than 30 institutions around the world, providing strong support for improving the accuracy of climate change predictions in the Huaihe River Basin [15]. Huang Xiaoyuan first selected five CMIP6 models with complete data based on previous achievements and used the bilinear interpolation method to uniformly interpolate the data with different resolutions to a grid of $0.5^\circ \times 0.5^\circ$ for the research [16]. To investigate the anticipated alterations in the characteristics of extreme precipitation in Guizhou Province due to climatic shifts, Feng Yelin conducted a comprehensive analysis of four distinct extreme precipitation indices at a spatial resolution of $0.5^\circ \times 0.5^\circ$, utilizing station-based observations in conjunction with daily precipitation datasets derived from five CMIP6 models [17]. This study delves into the spatiotemporal dynamics of both historical and prospective changes. As previously mentioned, the data derived from the CMIP6 simulations employed in the research exhibit a relatively low spatial and temporal resolution. When studying regions with rapidly changing environmental conditions, they cannot capture the local variability and nuances existing in the area. Therefore, they are unsuitable for extreme rainfall spatiotemporal changes that require fine-grained spatial information. For this reason, this paper uses high-resolution NEX-GDDP-CMIP6 experimental data for the research, which provides essential support.

The Huaihe River Basin is an important area for China's agriculture, but it is increasingly facing challenges created by climate change. Recent research shows that climate change affects various aspects of the environment, including the temperature, precipitation, and extreme weather events, affecting agricultural activities and production. For example, extreme temperatures have a negative impact on grain production in the Huaihe River Basin and the impact coefficient of extreme high temperatures on grain yield is -0.021 , which shows that yields decrease as temperatures increase [18]. This poses a major challenge to food security in the region. Climate change also promotes vegetation growth in watersheds while inhibiting vegetation growth in other areas [19]. It affects land-use

patterns, thereby affecting agricultural and industrial production outcomes in the Huaihe River Basin. In the context of climate change posing a major threat to agriculture and production activities in the Huaihe River Basin, the prediction of extreme precipitation in this study can effectively mitigate the impact of climate change while ensuring the smooth progress of agriculture and production activities.

Natural disasters are frequent in the Huaihe River Basin and the model resolution is an essential factor affecting the performance of precipitation simulation. The research meticulously selects and computes the pertinent extreme precipitation indices according to the comprehensive datasets from 45 meteorological stations from 1960 to 2014. Meanwhile, it analyzes the spatiotemporal variation characteristics of the Huaihe River Basin in the selected historical period (1960–2014). Then, we construct the Taylor diagram to visually evaluate the performance of multiple high-resolution NEX-GDDP-CMIP6 climate models in simulating the Huaihe River Basin's precipitation. We select the top-five models with the best performance averaging to calculate the extreme precipitation index so that we can analyze its spatiotemporal change features in the future period (2015–2100). It explores the impact of extreme precipitation indices on the precipitation changes to provide decision-making suggestions for flood warnings and agricultural development in the Huaihe River Basin.

2. Materials and Methods

2.1. Study Area

The Huaihe River Basin is between the Yangtze and Yellow Rivers in the eastern part of China (Figure 1). The geographical coordinates demarcate a region spanning from $111^{\circ}55'$ to $121^{\circ}25'$ in eastern longitude and encompassing $30^{\circ}55'$ to $36^{\circ}36'$ in northern latitude. The basin, originating from the western terrains of the Tongbai and Funiu Mountains, extends its boundaries to the eastern periphery of the Yellow Sea. To the south, it delineates its contours along the Yangtze River, complemented by the majestic Dabie Mountains, the undulating Jianghuai Hills, the intricate waterways of the Tongyang Canal, and the southern embankments of the Rutai Canal. Furthermore, its northern frontier is demarcated by the southern embankment of the Yellow River and the eminent Mount Tai, seamlessly adjoining the Yellow River Basin.

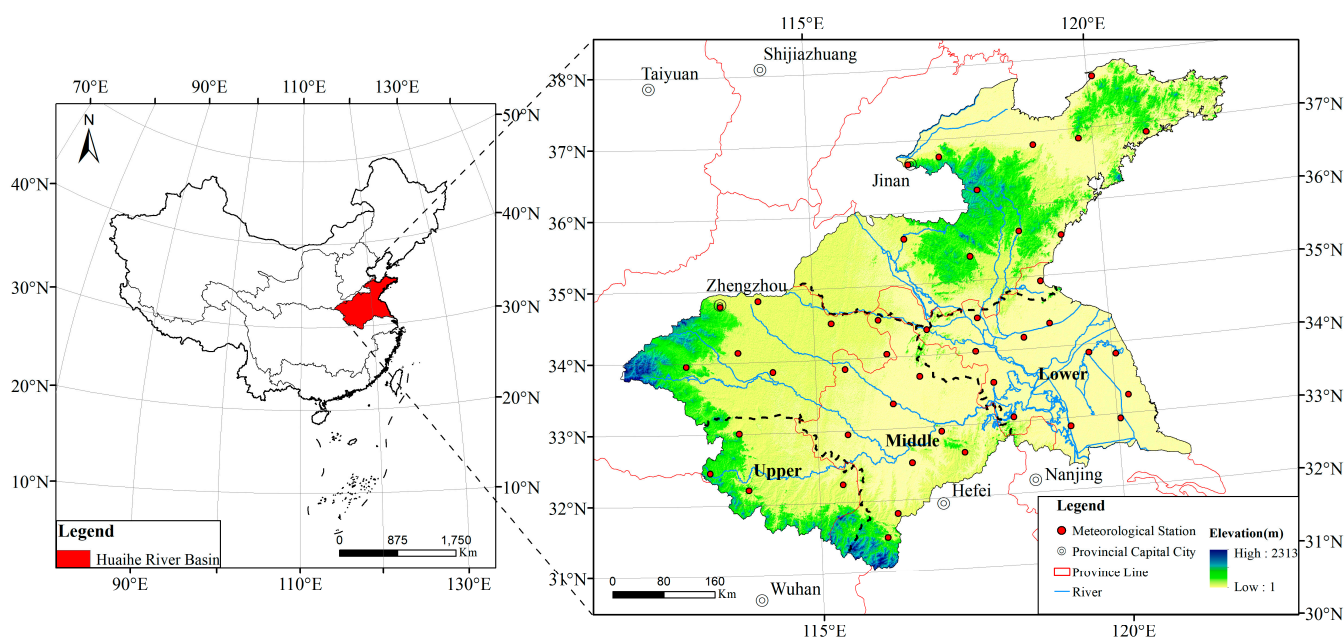


Figure 1. The spatial distribution of the Huaihe River Basin.

The Huaihe River Basin is in the transition zone from a subtropical humid climate to a warm temperate semi-humid climate. Due to the superimposed influence of multiple weather systems, the regional environment is changeable, and the weather changes drastically, leading to an uneven spatiotemporal rainfall distribution [20,21]. It has prominent seasonal characteristics, with high temperature and rain in summer and a low temperature and little rain in winter. The annual average precipitation is between 572.6 and 1278.8 mm in the basin. In the Huaihe River Basin, the precipitation is predominantly concentrated during the flood season, spanning from May to September, which accounts for approximately 63.8% of the annual precipitation. This pattern underscores a pronounced spatiotemporal heterogeneity in the annual precipitation distribution, a phenomenon observed in various river basins across China [22]. Most rainfall focuses on the primary flood season and the basin's southern part. The time and space distribution of precipitation within the year is unbalanced, and it is mostly concentrated in the main flood season and the southern part of the basin. Extreme or long-term continuous precipitation events can easily cause flood disasters, and it is a flood-prone area.

2.2. Data Source

This investigation predominantly employed two distinct categories of data: the first encompassed historically recorded climatic measurements, while the second were derived from future climatic projections sourced from NEX-GDDP-CMIP6.

2.2.1. Historically Measured Climate Data

This study's historical measured climate data was obtained from the daily dataset (V3.0) of China's national surface meteorological stations. The daily observation data of critical meteorological factors on the ground since January 1951, including the daily precipitation of 45 meteorological stations in the Huaihe River Basin, were distributed in Zhengzhou, Kaifeng, Baofeng, Xuchang, Xihua, Zhumadian, Xinyang, Tongbai, Shangqiu, Gushi, Longkou, Haiyang, Pingdu, Weifang, Rizhao, Jinan, Zhangqiu, Yiyuan, Juxian, Feixian, Yanzhou, Dangshan, Yongcheng, Bozhou, Fuyang, Huoshan, Luan, Shouxian, Dingyuan, Bengbu, Mengcheng, Suzhou, Xuzhou, Pizhou, Ganyu, Guanyun, Shuyang, Suining, Sihong, Xuyi, Gaoyou, Funing, Sheyang, Dafeng, and Dongtai. The period studied was 1960–2014 (Figure 2).

2.2.2. NEX-GDDP-CMIP6 Dataset

In the NEX-GDDP-CMIP6 dataset, 35 CMIP6 precipitation data nodes were converted into a streamlined resolution of precisely 0.25° by 0.25° using a sophisticated conversion mechanism. This intricate transformation was accomplished through 'downscaling', which facilitated a superior spatial resolution.

The dataset not only encompassed the historical data spanning from 1950 to 2014, but also integrated the data from four prospective scenarios. The shared socio-economic pathway (SSP) scenarios defined the diverse trajectories of the socio-economic evolution that influenced potential future climate scenarios. We designated these pathways as SSP1-2.6, SSP2-4.5, SSP3-7.0, and SSP5-8.5. Each pathway aligned with a distinct greenhouse gas concentration trajectory, with the subsequent number after the SSPs signifying the radiative forcing level anticipated by the century's conclusion.

We then used the data from these scenarios to perform extreme precipitation index analyses covering the period from 2015 to 2100. This forecast period allowed the researchers to analyze and predict the potential impacts of various climate change scenarios. Therefore, the NEX-GDDP-CMIP6 dataset is an essential tool for climatologists to model possible future climate conditions and their effects.

To ensure the data's integrity, we chose 13 models in this dataset, using 'r1i1p1f1' as the driver and 'gn' as the grid. The term 'r1i1p1f1' specified the specific model run, initialization method, physics version, and forcing used in each model, while 'gn' referred to the grid used for the model output. Integrating these sophisticated models, and the

distinct driver and grid infrastructure, provided a thorough and nuanced examination of the climate data. The detailed specifics of each model, the driver, the grid, and other essential information are neatly displayed in Table 1. By using this methodology, scholars can expediently cross-reference and incorporate the data into their empirical analyses, rendering the NEX-GDDP-CMIP6 dataset an indispensable cornerstone in climatological research.

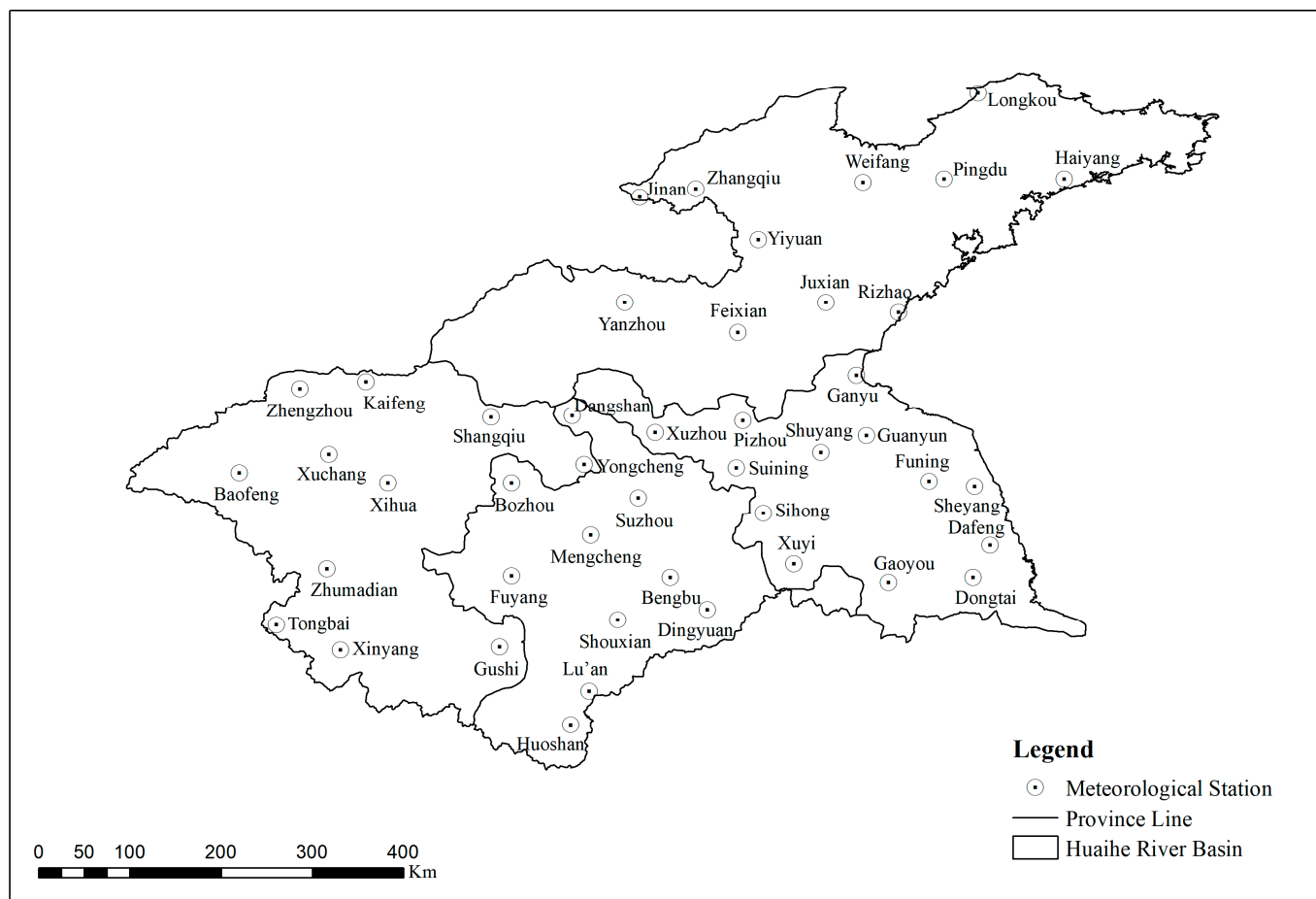


Figure 2. Distribution of 45 meteorological stations in the Huaihe River Basin.

Table 1. List of GCMs from the CMIP6 project considered in this study.

| Number | Model | Institution | Country | Resolution |
|--------|---------------|-------------|-----------|---------------|
| 1 | ACCESS-CM2 | ACCESS | Australia | 0.25° × 0.25° |
| 2 | ACCESS-ESM1-5 | ACCESS | Australia | 0.25° × 0.25° |
| 3 | BCC-CSM2-MR | BBC | China | 0.25° × 0.25° |
| 4 | CMCC-CM2-SR5 | CMCC | Italy | 0.25° × 0.25° |
| 5 | CMCC-ESM2 | CMCC | Italy | 0.25° × 0.25° |
| 6 | CanESM5 | CCCMA | Canada | 0.25° × 0.25° |
| 7 | MIROC6 | MIROC | Japan | 0.25° × 0.25° |
| 8 | MPI-ESM1-2-HR | MPI | Germany | 0.25° × 0.25° |
| 9 | MPI-ESM1-2-LR | MPI | Germany | 0.25° × 0.25° |
| 10 | MRI-ESM2-0 | MRI | Japan | 0.25° × 0.25° |
| 11 | NorESM2-LM | NCC | Norway | 0.25° × 0.25° |
| 12 | NorESM2-MM | NCC | Norway | 0.25° × 0.25° |
| 13 | TaiESM1 | RCEC | China | 0.25° × 0.25° |

2.3. Methods

2.3.1. Extreme Precipitation Index

The Intergovernmental Panel on Climate Change (IPCC) delineates extreme weather and climatic phenomena as instances where a particular meteorological or climatic variable surpasses (or falls below) a designated threshold, situated proximate to the uppermost (or lowermost) spectrum of its historically observed values [23]. In scientific research applications, meteorologists can quantitatively define extreme climate events. The manuscript delineates a threshold-based extreme climate index, which researchers ubiquitously employ to investigate extreme climatic phenomena. This index's versatility is underscored by its applicability across diverse regions and adaptability to myriad datasets, facilitating nuanced comparative analyses.

Table 2 shows the eight extreme precipitation indices recommended by the Expert Group on Climate Change Detection and Extreme Event Indices (ETCCDI) used in this study [24,25]. These indices can be divided into four categories: one is an absolute index, such as R10. The second is a relative index, such as PRCPTOT, R95p, and R99p. The third is an extreme value index, such as RX1day. The fourth is another index, such as CDD, CWD, and SDII.

Table 2. Introduction of extreme precipitation indices.

| Index | Abbreviation | Definition | Unit |
|-----------------------------|--------------|--|---------------------------------|
| Moderate rainy days | R10 | Number of days with daily precipitation ≥ 10 mm | d |
| Total annual precipitation | PRCPTOT | Cumulative precipitation with daily precipitation ≥ 1 mm | mm |
| Heavy precipitation | R95p | Annual cumulative precipitation with daily precipitation $> 95\%$ quantile | mm |
| Very heavy precipitation | R99p | Annual cumulative precipitation with daily precipitation $> 99\%$ quantile | mm |
| Maximum 1-day precipitation | RX1day | Maximum 1-day precipitation per month | mm |
| Consecutive dry days | CDD | The maximum continuous number of days with daily precipitation < 1 mm | d |
| Consecutive wet days | CWD | The maximum continuous number of days with daily precipitation > 1 mm | d |
| Precipitation intensity | SDII | The ratio of total annual precipitation to the number of wet days | $\text{mm} \cdot \text{d}^{-1}$ |

2.3.2. RclimDex Model

This paper employed the RclimDex model, a computation software grounded in the R language environment, to calculate the extreme climate index. The model conducts a rigorous examination and controls the data from the selected stations. We also executed rigorous temporal consistency analyses, eliminating the anomalous data points and erroneous values. Advanced measures were implemented, including assessing whether the daily minimum temperature surpassed the established maximum and executing rigorous extreme value analyses [26]. In the rare instances of missing data, we used the linear interpolation method to ensure data integrity and consistency.

The study utilized daily meteorological data from each station in the Huaihe River Basin and incorporated the precipitation data from the NEX-GDDP-CMIP6 dataset as the input for the model. The data from each meteorological station underwent rigorous corrections in a textual format. The data sequence accommodated omissions, designating any absent data with a value of -99.9 . We initially scrutinized the meteorological data for logical consistency during our comprehensive research. Following the completion of the verification phase, we employed a range of sophisticated computational methodologies, including machine learning algorithms, statistical models, and data mining techniques, to conduct a comprehensive analysis and the processing of the data. The RclimDex model played a pivotal role in this process by comprehensively analyzing the subsequent data through its multi-layered approach. Specifically, the software first segregated the data into various climate indices and parameters. It then applied advanced statistical tests to

identify patterns, trends, and anomalies within each index. Finally, the model synthesized these individual analyses to generate a holistic understanding of the climate variables under study, thereby ensuring a robust and nuanced interpretation of the data. This meticulous approach ensured the accuracy and reliability of our findings, providing a robust foundation for further scientific inquiries. By standardizing the treatment of the missing data, we aimed to maintain the integrity of our datasets, facilitating more consistent and meaningful interpretations.

2.3.3. Taylor Diagram

The Taylor plot, as introduced by Taylor in 2001, serves as a predominant technique for model evaluations [27]. This method predominantly harnesses three statistical metrics, the correlation coefficient, root mean square error (RMSE), and standard deviation ratio, facilitating a comprehensive assessment of the congruence or disparity between model simulations and empirical observations.

The Taylor plot critically incorporates the correlation coefficient, quantifying the linear relationship between two datasets. A heightened correlation coefficient underscores a robust linear association between the model simulations and the observed data, denoting an enhanced model accuracy. Conversely, the RMSE delineates the variance between the model's projected values and the actual observations. A diminished RMSE value indicates a minimal divergence between the model's forecasts and the observed data, implying a heightened model precision.

The standard deviation ratio emerges as a pivotal metric in the Taylor plot. Defined by the quotient of the model's standard deviation result and the observed data's standard deviation, this ratio elucidates the model's variability in the juxtaposition with the observed data. When the ratio approximates 1, it signifies a harmonious alignment of the model's variability with the observed data, thereby implying a model of heightened reliability. The graphical representation of the simulated point with the observed datum offers a visual interpretation of the model's simulation prowess. A proximate positioning of the bogus end to the designated marker on the Taylor plot infers the robust simulation capability of the model.

In the context of this paper, both the observational and model data underwent standardization procedures before being evaluated by the Taylor diagram. Standardization is crucial as it enables a fair comparison between the two sets of data by nullifying the potential influence of differing scales and units. This comprehensive evaluation using the Taylor plot thus aided in verifying the validity and reliability of the model under consideration.

2.3.4. Sen+Mann–Kendall Trend Analysis

Sen's trend analysis robustly withstands the influence of outliers and operates independently of any specific distribution adherence. It adeptly circumvents measurement inaccuracies and discrete data variances, finding extensive application in climatological and hydrological sequence evaluations [28]. In this paper, the Sen trend was used to analyze the change in the extreme precipitation index in the Huaihe River Basin, and the Mann–Kendall method was used to test the significance of the changing trend [29]. The specific calculation formula is as follows:

$$\beta = \text{Median}\left(\frac{x_j - x_i}{j - i}\right), \forall j > i \quad (1)$$

In the formula, β is the changing trend of the extreme precipitation index; i and j are the positions in the time series, respectively, representing the extreme precipitation index value of the i and j th times. When $\beta > 0$, the extreme precipitation index is on the rise; $\beta < 0$ indicates that the extreme precipitation index is on a downward trend.

3. Results

3.1. Taylor Diagram Climate Model Evaluation

Figure 3 comprehensively evaluates the Huaihe River Basin's precipitation patterns from 1960 to 2014, as simulated by 13 global models from the Coupled Model Intercomparison Project Phase 6 (CMIP6). A key metric used in this evaluation was the spatial correlation coefficient, which measured the degree of correlation between the simulated results of these models and the actual observational data gathered within the Huaihe River Basin during the same period. Each of the 13 models demonstrated a spatial correlation coefficient higher than 0.69 and the top-five values were all higher than 0.74 [30]. This strong correlation reflects the models' ability to accurately replicate the spatiotemporal distribution characteristics of precipitation.

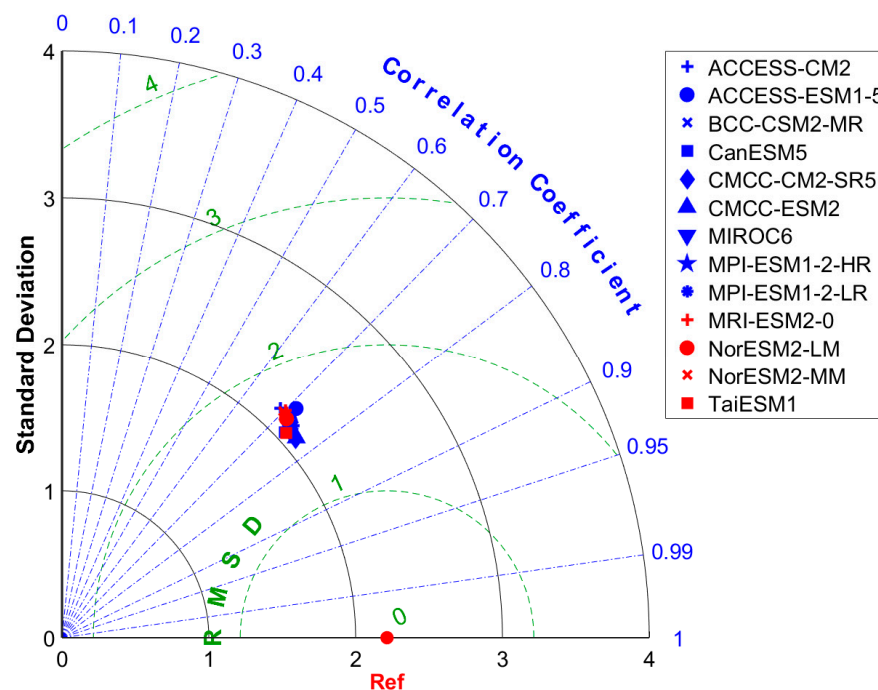


Figure 3. Taylor plots of the average precipitation in the Huaihe River Basin simulated by 13 CMIP6 global models in the historical period (1960–2014).

The results across the different models are notably consistent, with each demonstrating a similar level of accuracy. This consistency suggests that researchers can reliably use these CMIP6 models to simulate precipitation patterns in the Huaihe River Basin. The Taylor plot evaluation identified the top-five performing models as CMCC-CM2-SR5, CMCC-ESM2, TaiESM1, MPI-ESM1-2-LR, and CanESM5. We then averaged these five models to obtain an optimal representation of precipitation in the Huaihe River Basin during the future period. Because future climate change may not follow a single climate pattern, it prefers focusing on using multiple climate models. It can help reduce the uncertainty caused by assessing a single climate model, making the analysis results more reliable and reasonable.

3.2. Spatiotemporal Distribution Characteristics of Extreme Precipitation Indices in the Huaihe River Basin in the Historical Period

3.2.1. Temporal Variability of the Extreme Precipitation Index in the Huaihe River Basin in the Historical Period

The data collected from 1960 to 2014 illustrate the interannual variation trend of the extreme precipitation event indices in the Huaihe River Basin, as shown in Figure 4. During these 55 years, several indices of extreme precipitation in the Huaihe River Basin exhibit an upward trend, including 10 mm precipitation days (R10), annual total precipitation (PRCP-

TOT), extreme precipitation (R95p), and extreme heavy precipitation (R99p). The trend coefficients for these indices are 0.07 d/10 a, 1.38 mm/10 a, 5.76 mm/10 a, and 0.32 mm/10 a. However, these trends do not pass the significance test at a 95% confidence level.

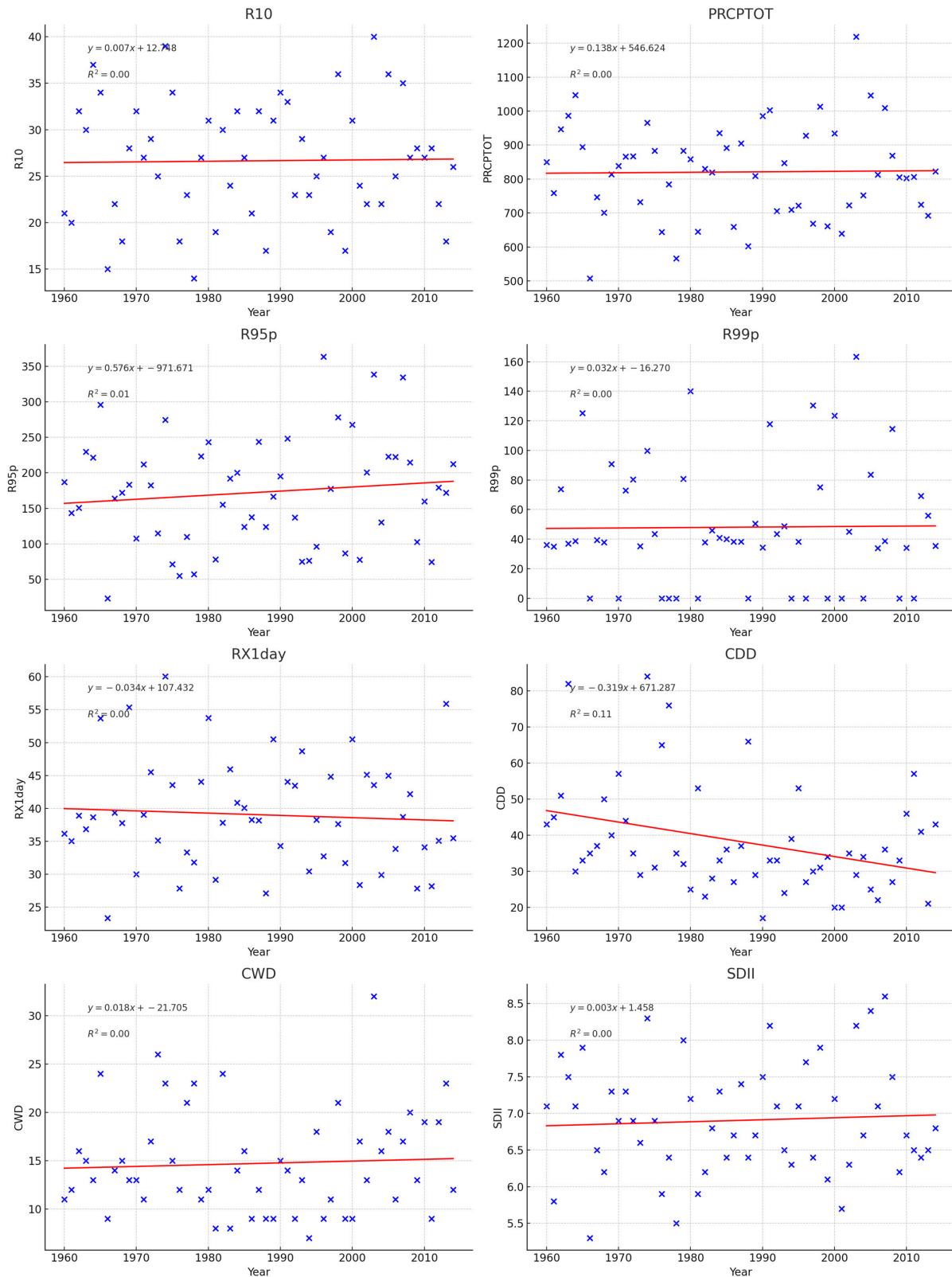


Figure 4. Temporal variability of extreme precipitation index in the Huaihe River Basin in the historical period.

The interannual oscillations of the extreme precipitation event index within the Huaihe River Basin exhibited a nuanced augmentation, though its prominence remained statistically inconsequential. Interestingly, the 1-day maximum precipitation (RX1day) revealed a downward trend with a coefficient of -0.34 mm/10 a. However, similar to the upward trend, this trend did not pass the significance test at a 95% confidence level.

On the one hand, the analysis also revealed a downward trend in consecutive dry days (CDD) with a -3.19 d/10 a trend coefficient. In contrast to the other movements, this trend passed the significance test at a 95% confidence level, indicating a statistical significance. On the other hand, consecutive wet days (CWD) and average daily precipitation intensity (SDII) demonstrated an upward trend. The trend coefficients for these indices were 0.18 d/10 a and 0.03 mm/day/10 a, respectively. Nonetheless, neither of these trends passed the significance test at the 95% confidence level.

In conclusion, the study of the interannual variation trends of extreme precipitation event indices in the Huaihe River Basin from 1960 to 2014 revealed mixed results. Similarly, while the downward trend in the CDD index was statistically significant, the correlation was low. Further research may be needed to understand the implications of these trends.

3.2.2. Spatial Distribution of the Extreme Precipitation Index in the Huaihe River Basin in the Historical Period

Figure 5 shows that the historical period data from the rainfall observation stations are interpolated by the Kriging interpolation method. There were 45 observation stations in this area, which were dense enough and basically evenly distributed. Figure 5 delineates the spatial distribution of extreme precipitation indices across various monitoring stations from 1960 to 2014. These data convey distinct trends across the regions, underlining the diverse climatic conditions in the territories analyzed. An intriguing observation was the increasing trend of most extreme precipitation indices, barring the consecutive dry days index, as one transition from the northwest to southeast. In contrast, the CDD diminished in the same direction, indicating frequent dry spells in the northwest compared to the southeast.

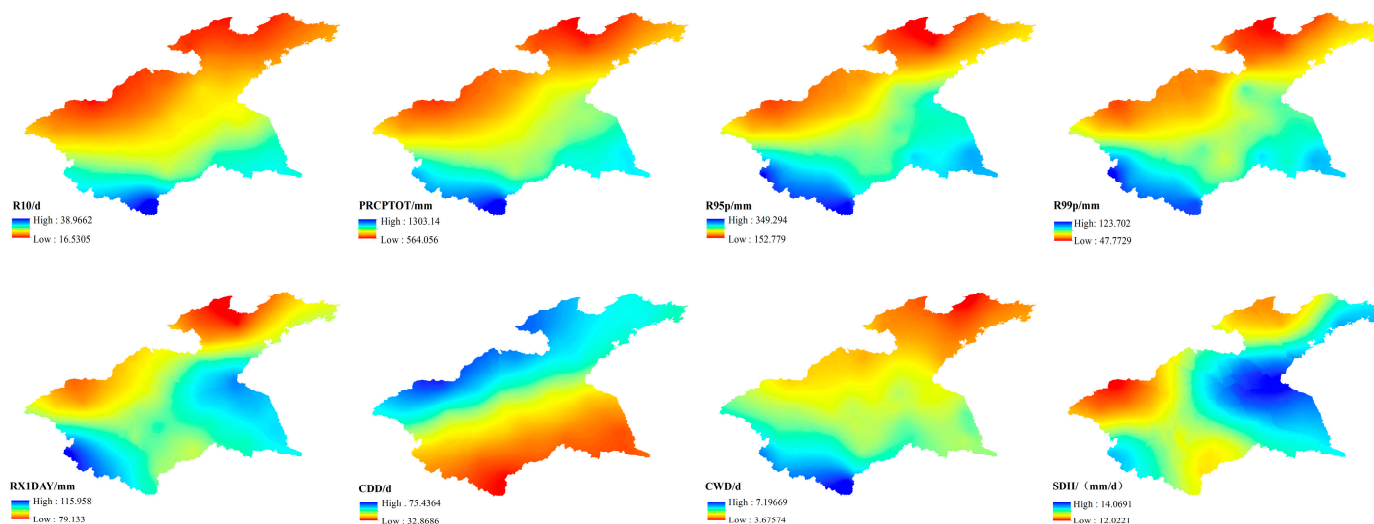


Figure 5. Spatial distribution of extreme precipitation indices in the Huaihe River Basin in the historical period.

Upon greater scrutiny, the days marked by a precipitation level of 10 mm or higher reveal a gradual increase from northwest to southeast. This growth peaks near the southwest Huaihe River Basin, indicating a heightened frequency of such rain events. In this context, the zenith of this trend lies southwest, implying optimal rainfall for agricultural endeavors. The R95p and R99p indices, symbolizing the cumulative rainfall on days exceeding the 95th and 99th percentiles of a standard period, respectively, exhibit a pronounced surge from

the northwest to southeast. It is noteworthy that R99p witnesses a swifter surge relative to R95p, with its apex observed around the central and southwestern sectors of the Huaihe River Basin, indicating this area's vulnerability to extreme rainfall episodes.

Moreover, the daily pinnacle precipitation showcased an analogous uptrend from the northwest to southeast. However, its main concentration was observed in the southeast and southwest of the Huaihe River Basin, hinting at a higher propensity for severe rainstorms in these locales. Contrarily, the prevalence of continuous dry days exhibited an incline from the southeast to northwest, standing in stark juxtaposition to the other precipitation markers. The southeast quadrant of the Huaihe River Basin witnessed a drastic reduction in consecutive dry days compared to the northwest, highlighting the former's humid climate against the latter's aridity.

A noteworthy point of contention emerged from the pronounced discrepancy between the frequency of continuously wet days and perpetually dry days. As one navigates from the northwest to southeast, this divergence accentuates, peaking in the southwest. Such a trend insinuates that the southwestern belt of the Huaihe River Basin retains a persistently moist climate on a year-round basis. Conclusively, the Huaihe River Basin's average daily precipitation intensity intensifies from the west to east. While a marginal escalation is evident in the southwest, the core remains eastward, emphasizing the region's geographical nuances that foster more intense rainfall in the east.

In the context of climatological discrepancies, it is crucial to highlight that while the models may suggest trends in extreme precipitation, on-the-ground observations can sometimes differ. The variations between the model projections and actual measurements can be attributed to various factors, including inherent model biases, changing land-use patterns, and localized climatic influences. In the given data, although we see a clear pattern in the precipitation indices, it is essential to corroborate these findings with climatological models to ensure accuracy and achieve a holistic understanding of extreme precipitation phenomena in the region.

3.3. Spatiotemporal Distribution Characteristics of Extreme Precipitation Index in the Huaihe River Basin in the Future

3.3.1. Distributions of Temporal Variability of Extreme Precipitation Indices in the Huaihe River Basin in the Future Period

Figure 6 compares various indicators of extreme precipitation indices. When analyzing various climate indices, specific patterns emerge across different scenarios. All scenarios exhibited similar distributions for the indices R10, RX1day, and SDII, with their median values being similar. SSP3-7.0 and SSP5-8.5 tended to have more comprehensive interquartile ranges in several indices, suggesting more variability. Specifically, SSP3-7.0 consistently showed higher medians in the indices related to precipitation extremes, such as R95p, R99p, and RX1day, anticipating of more severe rain events. SSP1-2.6 often presents tighter distributions, hinting at a potentially more stable or less variable climate in the indices considered.

SSP3-7.0 and SSP5-8.5 also forecasted more consecutive dry days, as the CDD index indicated the possibility of more prolonged dry spells. In contrast, SSP1-2.6 generally predicted a more consistent climate, as evidenced by its narrower interquartile ranges in several indices. The distributions for the CWD across all scenarios were relatively similar, but SSP2-4.5 and SSP3-7.0 showed slightly elevated medians. While the medians for some indices across the scenarios might appear comparable, the variability, as represented by the interquartile ranges, can be notably different.

It is crucial to contextualize these findings within the broader climate modeling framework. These scenarios are grounded in distinct assumptions about future socio-economic pathways, each with implications for climate change and its subsequent impacts. The observed differences in the indices across the various scenarios are a testament to these underlying assumptions and the diverse potential future scenarios they represent.

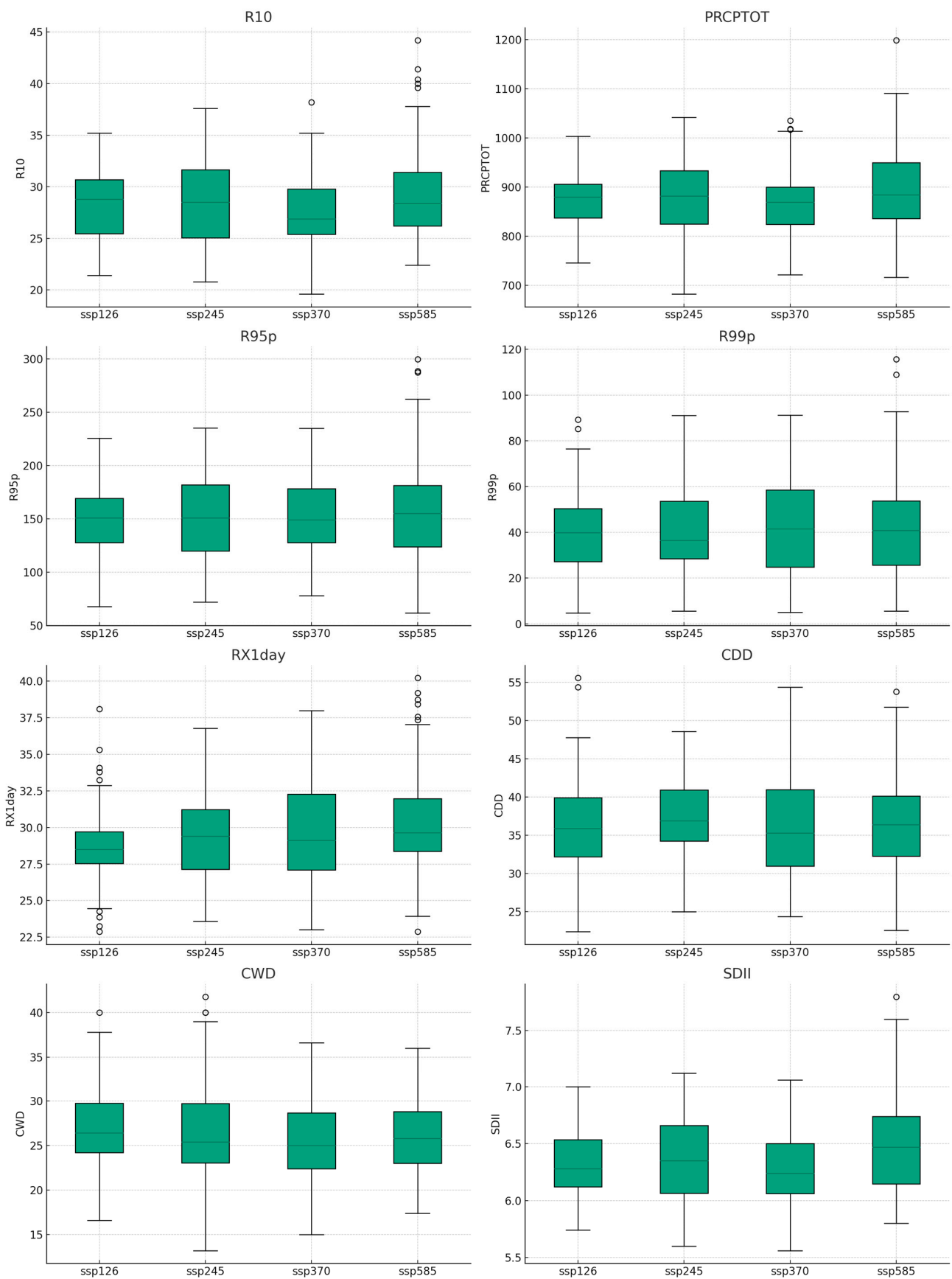


Figure 6. Distributions of temporal variabilities of extreme precipitation indices in the Huaihe River Basin in the future period.

3.3.2. Spatial Distribution of Extreme Precipitation Indices in the Huaihe River Basin in the Future Period

It can be seen from Figure 7 that there are significant differences in the variation trends of different extreme precipitation indices from 2021 to 2100. At the same time, a1, a2, a3, and a4 represent the spatial distributions of the relative change rates of each scenario in the short-term future (2021–2045). The values of b1, b2, b3, and b4 represent the mid-term future scenarios (2046–2070). The values of c1, c2, c3, and c4 represent the long-term future scenarios (2076–2100).

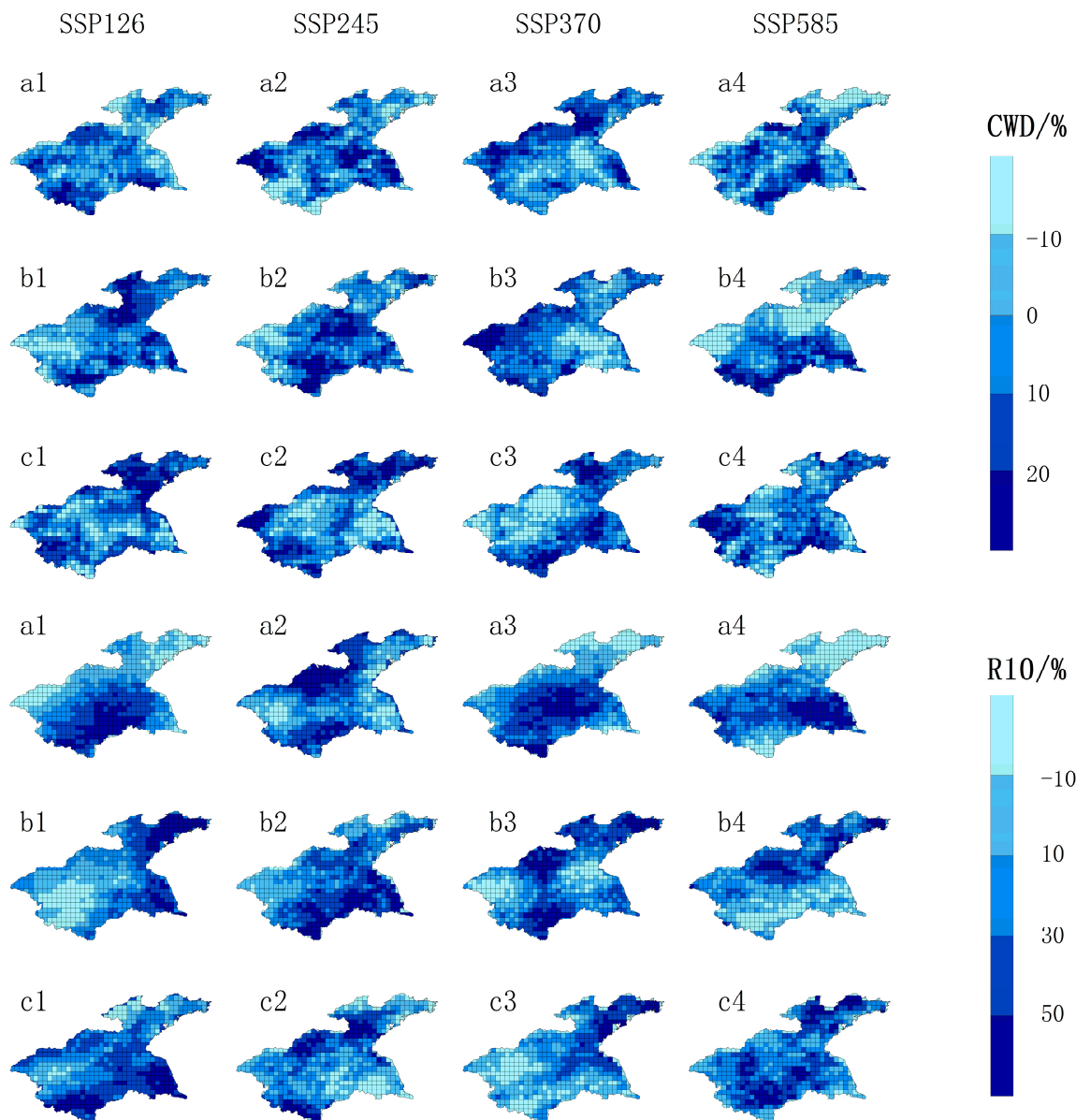


Figure 7. Cont.

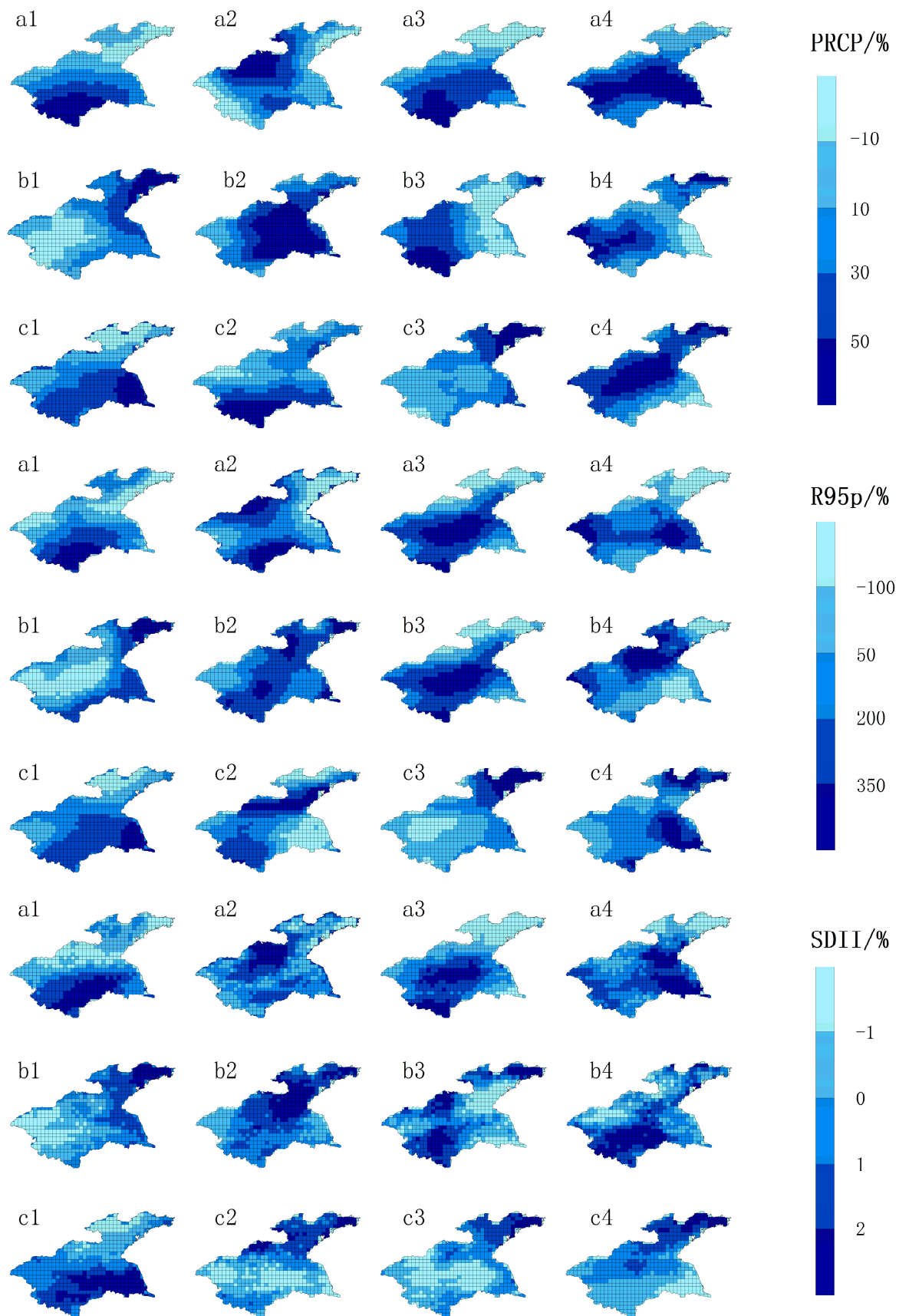


Figure 7. Spatial distribution of extreme precipitation indices in the Huaihe River Basin in the future period.

(1) Short-term future

The CWD shows an increasing trend in areas where SSP1-2.6 exceeds 93.6% and SSP3-7.0 exceeds 67.6%, mainly concentrating in the northern and eastern parts of the Huaihe River Basin. However, some places in the central and southern regions maintain a decreasing trend. Areas where SSP2-4.5 exceeds 85.9% and SSP5-8.5 surpasses 68.6% also show an increasing trend, mainly concentrating in the middle of the basin, while other regions maintain a steady or decreasing trend.

R10 shows an increasing trend in areas where SSP1-2.6 exceeds 89.8% and SSP3-7.0 exceeds 78.9%. It primarily maintains a rising trend in the central and southern parts of the Huaihe River Basin and a decreasing trend elsewhere. In the scenario of SSP2-4.5, an upward trend is discernible in over 56.7% of the areas under consideration, with a conspicuous concentration in the north and south, whereas the east and west exhibit a relatively diminished presence. In the scenario of SSP5-8.5, a substantial proportion, specifically exceeding 84.3%, of the regions exhibit a growth trend. This expansion primarily manifests in the eastern and western sectors, while it remains noticeably less prevalent in the northeast and southwest areas.

PRCPTOT shows an increasing trend in areas where SSP1-2.6 exceeds 95.9% and SSP3-7.0 exceeds 86.4%. The increase is primarily concentrated in the southern part, while other regions show a decreasing trend. Areas where SSP2-4.5 exceeds 86.5% also show an increasing trend. The growth focuses on the northern part of the basin in the middle, while other sites decrease. The places where SSP5-8.5 exceeds 87.7% show an increasing trend and the growth area becomes horizontal in the middle of the basin.

R95p shows an increasing trend in areas where SSP1-2.6 exceeds 87.7% and SSP3-7.0 exceeds 78.7%, mainly in the southwest of the Huaihe River Basin, while other regions show a decreasing trend. The increasing trend in areas where SSP2-4.5 exceeds 56.7% favors more north–south and fewer east–west sites. In contrast, areas where SSP5-8.5 exceeds 85.9% show a rising trend, with the growing areas concentrating more in the east and west.

SDII shows an increasing trend in areas where SSP2-4.5 exceeds 36.7% and SSP5-8.5 exceeds 90.6%, offering a growing trend in most regions in the Huaihe River Basin. The regions where the value of SSP1-2.6 surpasses 91.8% exhibit an ascending trajectory. The distribution tends to be more visible in the south and less in the north; the areas where SSP3-7.0 exceeds 69.7% indicate a growing trend and are more concentrated in the central part of the basin and the southwest region, while the northeast region maintains a decreasing trend.

(2) Mid-term future

The CWD shows an increasing trend in areas where SSP1-2.6 exceeds 46.6% and SSP3-7.0 exceeds 58.9%, revealing a distribution state with a significant change rate in the east and west. Areas with SSP5-8.5 exceeding 71.2% show an increasing trend. The distribution state shows a considerable change rate in the north and south. The areas with SSP2-4.5 exceeding 90.5% indicate a growing trend and the places with higher growth rates are concentrated in the central and eastern regions of the Huaihe River Basin. In contrast, the change rates in other areas are negative.

R10 shows an increasing trend in areas where SSP1-2.6 exceeds 58.9% and a growing trend in areas where SSP3-7.0 exceeds 73.1%. There is an expanding trend in areas where SSP5-8.5 exceeds 84.5%. The former is rainy in the east and west and the latter is rainy in the north and south. In SSP2-4.5, more than 91.8% of the parts show an increasing trend, and all areas except the northwest are rainy.

In SSP1-2.6, PRCPTOT shows an increasing trend in more than 59.7% of the regions. In SSP2-4.5, the whole basin's PRCPTOT shows a growing trend, the east–west distribution is maintained, and the total annual precipitation in the east is higher than that in the west and central east. In the SSP3-7.0 scenario, there is a noticeable augmentation in the PRCPTOT, an enhancement that permeates more than 79.1% of the assessed regions. In SSP5-8.5, PRCPTOT shows an increasing trend in more than 98.6% of the areas. Under these two

scenarios, the total annual precipitation in the basin's western area is significantly more than in the east.

In the SSP1-2.6 scenario, there was a noticeable ascending trajectory for the R95p indicator, prevalent in over 57.0% of the regions under consideration. Similarly, within the context of the SSP3-7.0 scenario, this particular metric illustrates an escalating pattern, observable in more than 72.1% of the investigated territories. And the regional distribution is the opposite. The specific performance is that the former offers a decreasing trend in the central area of the basin, while the latter shows an increasing trend in the leading site. In SSP2-4.5, more than 92.1% of the regions showed a rising trend of R95p, mainly showing a growing trend in all areas, except the west. The divergence from the R95p model was observed across more than 88.1% of the geographical territories delineated in the SSP5-8.5 scenario, thereby signifying an increasing trend. Remarkably, the northern sectors predominantly localized this amplification.

SDII showed an increasing trend in regions exceeding 40.6% in SSP1-2.6. In SSP2-4.5, SDII increased in more than 99.3% of the areas. The parts with the greatest intensities were all in the northeast of the Huaihe River Basin and the other areas of the whole region were higher. In SSP5-8.5, SDII maintained an increasing trend in more than 98.1% of the areas and a rising trend across the entire basin. But, in the northwest part, the indicator decreased. In SSP3-7.0, more than 92.1% of the regions increased the SDII values and they were concentrated in the north and south of the basin, while other areas were relatively flat or reduced.

(3) Long-term future

In SSP1-2.6, SSP2-4.5, and SSP5-8.5, more than 46.7%, 59.8%, and 58.3%, respectively, of the regions showed an increasing trend of the CWD and they were all in the northeast and southwest parts of the Huaihe River Basin. In SSP3-7.0, more than 65.3% of the regions showed an increasing CWD trend, excluding the watershed's northwestern part.

R10 showed an increasing trend in more than 53.9% of the regions in SSP1-2.6. In SSP5-8.5, more than 97.2% of the parts maintained growth. In general, most areas of the Huaihe River Basin showed an increasing trend and only a few places in the north and west maintained a decreasing trend. In scenario SSP2-4.5, the R10 index increased in more than 87.9% of the regions. It was mainly distributed in the north and south and showed a decreasing trend in the central part. In SSP3-7.0, a substantial majority, precisely 90.4% of the regions, witnessed an ascendant trend. We predominantly observed this upward trajectory in the eastern sectors and other significant areas.

PRCPTOT showed an increasing trend in more than 37.7% of the regions in scenario SSP1-2.6 and more than 91.8% of the areas in SSP2-4.5. All of them were concentrated in the southeast and southern regions, while other parts showed a decreasing trend. In SSP3-7.0, PRCPTOT increased in all areas, with the highest increase concentrated in the northeast of the basin. In SSP5-8.5, PRCPTOT also increased in more than 95.7% of the regions and the areas with increasing precipitation levels became the northern and western basins.

R95p increased in over 58.3% of the regions in the SSP1-2.6 scenario, showing a decreasing trend from south to north. In SSP2-4.5, around 96.2% of the regions experienced an increase, primarily in the northern and southwestern areas. More than 91.8% of the areas in the SSP3-7.0 scenario showed an increase, with growth mainly observed in the northeastern region. In SSP5-8.5, over 99.6% of the areas exhibited an increasing trend, covering the entire Huaihe River Basin.

SDII displayed an increasing trend in areas where SSP1-2.6 exceeded 34.8%, with a decreasing trend from south to north. Conversely, in the SSP5-8.5 scenario, the trend was reversed, showing an increasing trend in areas exceeding 98.9% and a decreasing trend from north to south; in regions where SSP2-4.5 and SSP3-7.0 surpassed 88.1% and 82.4%, an increasing trend was observed, with the growth concentrated in the northern and northeastern areas.

4. Discussion

4.1. Model Evaluation and Historical Analysis

Using the Taylor diagram to evaluate the performance of various climate models is a practical approach widely adopted in climate studies [31]. The high-spatial-correlation coefficient of over 0.69 across 13 global models from CMIP6 is noteworthy and indicates the reliability of these models in simulating precipitation patterns. The supplementary literature shows a spatial correlation coefficient of 0.69, indicating reasonable accuracy values [32]. As a result, the findings strengthen their credibility and align with other studies that report the good performance of CMIP6 models across various geographical settings [33]. Further bolstering the credibility of the findings is the consistency across models. The selection of the top-five models with values higher than 0.74, namely, CMCC-CM2-SR5, CMCC-ESM2, TaiESM1, MPI-ESM1-2-LR, and CanESM5, provides a robust representation of future predictions. Climate models have been used in the Huaihe River Basin to understand hydrological responses under different scenarios.

A comparison of the historical data between 1960 and 2014 shows historical trends. While several indices of extreme precipitation exhibit an upward trend, their statistical significance remains inconclusive. The only exception is the CDD, which shows a statistically significant downward trend. As a result, extreme rainfall events are occurring more frequently, while dry days are decreasing. There are implications for both agriculture and infrastructure in the Huaihe River Basin due to this complex scenario. On the one hand, increased extreme precipitation can lead to flooding, affecting agriculture and infrastructure. On the other hand, a decrease in dry days might benefit agriculture, but can also lead to waterlogging issues.

Using Taylor diagrams and a high-spatial-correlation coefficient validates the effectiveness and reliability of the selected climate models. In the Huaihe River Basin, these models offer valuable insights into precipitation patterns and their potential impacts, which are necessary for future planning and risk management.

4.2. Spatial Variation and Regional Disparities

With its intricate climatic tapestry, the Huaihe River Basin reveals itself through the spatial distribution of extreme precipitation indices. A discernible increasing trend characterizes most of these indices, transitioning from the northwest to southeast, except for the CDD. This pattern underscores the heightened vulnerability of the southeastern region to extreme rainfall events, presenting potential challenges and considerations for flood management and agricultural strategies. Conversely, the southwest direction of the basin emerges as a beacon of agricultural promise. The consistent and higher frequency of rainfall events in this quadrant attests to its natural predisposition for crop cultivation. It emphasizes the region's advantage, fortified by its generous rainfall. This intricate spatial variation underscores the need for region-specific strategies and interventions, ensuring that each area harnesses its climatic strengths while mitigating potential vulnerabilities.

4.3. Future Projections and Implications

It is important to note that the current study did not delve into how the circulation systems responded to weather changes. While the projections spanning from 2015 to 2100 offer valuable insights into potential future trends in rainfall events and their impacts on the Huaihe River Basin, the study is limited in its scope concerning atmospheric circulation systems. These systems play a crucial role in weather patterns and understanding their responses to changing climatic conditions can provide a more holistic view of the challenges and opportunities that lie ahead.

The projections spanning from 2015 to 2100 hold profound significance for understanding the future of climate change and its impact on various sectors. By analyzing a range of scenarios, such as SSP1-2.6, SSP2-4.5, SSP3-7.0, and SSP5-8.5, the study provided a comprehensive understanding of the potential future trends in the Huaihe River Basin. The evidence gathered indicates the potential intensification of rainfall events, most notably

within the parameters of the SSP3-7.0 scenario. This has far-reaching implications for the region's strategic approaches to flood management, infrastructural advancements, and agronomic methodologies. Furthermore, the study revealed that the future distribution characteristics of precipitation patterns were not uniform across the region. Regional disparities were evident, with indices, such as CWD, R10, PRCPTOT, R95p, and SDII, showing an upward trajectory in the basin's northeastern, southwestern, and southeastern sectors. This suggested the potential intensification of precipitation and protracted wet durations in these specific locales. Such a climatic shift presents a dichotomy of outcomes: on the one hand, augmented rainfall can benefit agricultural endeavors; yet, on the other, it introduces complexities in water stewardship, flood mitigation, and infrastructural resilience strategies.

Future research should focus on studying how circulation systems respond to weather changes in the Huaihe River Basin for a more in-depth understanding of the subject matter. This can involve the use of advanced climate models that incorporate atmospheric circulation patterns, as well as ground-based observations to validate these models. The researchers can also explore the interplay between circulation systems and other climatic variables, such as temperature and humidity, to achieve a more holistic understanding of weather patterns. Additionally, the long-term monitoring of circulation systems can provide valuable data for assessing their stability and adaptability in the face of changing climatic conditions. By integrating these elements into future studies, researchers can offer more comprehensive strategies for flood management, water stewardship, and infrastructural planning systems, thereby contributing to the region's long-term sustainability.

4.4. Agricultural Production and Flood Safety

The study's findings underscore the need for region-specific and dynamic adaptation strategies in the Huaihe River Basin, particularly for agricultural production and flood safety. In agricultural production, the spatial and temporal variations in extreme precipitation indices, like CWD and SDII, suggest that different regions within the basin require tailored approaches. For instance, the increasing trend in the CWD in the northern and eastern parts may necessitate a shift towards adopting water-intensive crops. In contrast, the decreasing trend in the central and southern regions calls for drought-resistant varieties and efficient irrigation systems.

Regarding flood safety, an upward trajectory in extreme precipitation indices, such as R10 and R95p, across multiple scenarios indicates that flood risks are imminent, especially in the central and southern parts of the basin. Consequently, immediate and long-term measures are needed, including improved flood forecasting systems and sustainable land-use practices. Given the evolving nature of these trends, it is crucial for the future research to integrate these climatic projections with the socio-economic factors and to continually update the adaptation and mitigation strategies as new data become available.

5. Conclusions

Utilizing the observational data from 45 meteorological stations situated in the Huaihe River Basin spanning the period from 1960 to 2014, in conjunction with the NEX-GDDP-CMIP6 precipitation model dataset, we conducted a comprehensive analysis of the spatiotemporal variation attributes of the extreme precipitation index for both historical and projected future intervals, employing sophisticated methodologies, including the Taylor diagram and trend analysis techniques. The main conclusions are as follows:

(1) Over the past 55 years, the interannual variation trend of the extreme precipitation event index in the Huaihe River Basin is yet to be made apparent. There is only a slight but statistically insignificant increase. Spatially, except for the CDD, the extreme precipitation indices show a gradual increase from the northwest to southeast, while the CDD exhibits a decreasing trend from the northwest to southeast.

(2) Under the same scenario in the future, the rate of change of each index will continue to increase over time. Spatially, the future increase in extreme precipitation in the Huaihe

River Basin will exhibit a spatial variation characteristic that decreases from the northwest to southeast. With the evolution of different scenarios, we anticipate a gradual escalation in the annual and excessive precipitation growth rates. Moreover, as time unfolds, the disparity between these varied scenarios is expected to amplify significantly. Additionally, the intensity of extreme precipitation may increase in the southeast of the Huaihe River Basin.

(3) CWD, R10mm, PRCPTOT, R95p, and SDII are the leading indices that affect extreme precipitation changes in the Huaihe River Basin. Judging from the performance of these indicators on the map, the northeast, southwest, and southeastern parts of the Huaihe River Basin will experience higher precipitation levels and longer wet periods for most of the forecasted subsequent 80 years. In other regions, the rainfall scenario will vary significantly in different periods.

Author Contributions: Conceptualization, data collection, formal analysis, writing—original draft preparation: M.T.; writing—review and editing, supervision: L.L., Z.L. and Z.T. All authors have read and agreed to the published version of the manuscript.

Funding: This research was funded by the fund of Henan Province Fund (Research on flood risk information technology) (Grant No. 232102320002) and the National Natural Science Foundation of China (Grant No. 42101383).

Data Availability Statement: The data that support the findings of this study are available from the corresponding author upon reasonable request. Some data are not publicly available due to privacy or ethical restrictions. The data that are publicly available can be found in the NCCS (<https://www.nccs.nasa.gov/services/data-collections/land-based-products/nex-gddp-cmip6> (accessed on 25 October 2023)) and Google Scholar (<https://scholar.google.com.hk/?hl=en> (accessed on 25 October 2023)).

Acknowledgments: We want to express our deepest gratitude to the faculty and staff of the School of Earth Science and Technology, Zhengzhou University, for their invaluable guidance and support throughout the research process. Special thanks to the academic team for their tireless effort to ensure the smooth progress of the project from the initial proposal to the final paper submission stages. We also thank Leilei Li, Zhi Li, and Zhihui Tian for the technical support, whose expertise was instrumental during this study's data collection and analysis phases. In addition, we would also like to thank the Henan Province Fund for its generous donation of materials and resources, which significantly contributed to the successful completion of our experiments. Lastly, we express our gratitude to our peers and colleagues who provided constructive feedback and moral support during the research process.

Conflicts of Interest: The authors declare no conflict of interest.

References

1. Adopted, I.P.C.C. *Climate Change 2014 Synthesis Report*; IPCC: Geneva, Switzerland, 2014; pp. 1059–1072.
2. Xu, D.; Liu, D.; Yan, Z.; Ren, S.; Xu, Q. Spatiotemporal variation characteristics of precipitation in the Huaihe River Basin, China, as a result of climate change. *Water* **2023**, *15*, 181. [[CrossRef](#)]
3. Lin, H.; Wang, J.; Li, F.; Xie, Y.; Jiang, C.; Sun, L. Drought trends and the extreme drought frequency and characteristics under climate change based on SPI and HI in the upper and middle reaches of the Huai River Basin, China. *Water* **2020**, *12*, 1100. [[CrossRef](#)]
4. Khaing, Z.M.; Zhang, K.; Sawano, H.; Shrestha, B.B.; Sayama, T.; Nakamura, K. Flood hazard mapping and assessment in data-scarce Nyaungdon area, Myanmar. *PLoS ONE* **2019**, *14*, e0224558. [[CrossRef](#)] [[PubMed](#)]
5. Wang, G.; Zhang, Q.; Yu, H.; Shen, Z.; Sun, P. Double increase in precipitation extremes across China in a 1.5 °C/2.0 °C warmer climate. *Sci. Total Environ.* **2020**, *746*, 140807. [[CrossRef](#)] [[PubMed](#)]
6. Allan, R.P.; Soden, B.J. Atmospheric warming and the amplification of precipitation extremes. *Science* **2008**, *321*, 1481–1484. [[CrossRef](#)]
7. Yazdandoost, F.; Moradian, S.; Izadi, A.; Aghakouchak, A. Evaluation of CMIP6 precipitation simulations across different climatic zones: Uncertainty and model intercomparison. *Atmos. Res.* **2021**, *250*, 105369. [[CrossRef](#)]
8. Masson-Delmotte, V.; Zhai, P.; Pirani, A.; Connors, S.L.; Péan, C.; Berger, S.; Caud, N.; Chen, Y.; Goldfarb, L.; Gomis, M.I.; et al. *Climate Change 2021: The Physical Science Basis. Contribution of Working Group I to the Sixth Assessment Report of the Intergovernmental Panel on Climate Change*; Cambridge University Press: Cambridge, UK; New York, NY, USA, 2021; Volume 2.

9. Shahi, N.K.; Das, S.; Ghosh, S.; Maharana, P.; Rai, S. Projected changes in the mean and intra-seasonal variability of the Indian summer monsoon in the RegCM CORDEX-CORE simulations under higher warming conditions. *Clim. Dyn.* **2021**, *57*, 1489–1506. [[CrossRef](#)]
10. Shahi, N.K.; Rai, S.; Verma, S.; Bhatla, R. Assessment of future changes in high-impact precipitation events for India using CMIP6 models. *Theor. Appl. Climatol.* **2023**, *151*, 843–857. [[CrossRef](#)]
11. Yao, Y.; Qu, W.; Lu, J.; Cheng, H.; Pang, Z.; Lei, T.; Tan, Y. Responses of hydrological processes under different shared socioeconomic pathway scenarios in the Huaihe River Basin, China. *Water* **2021**, *13*, 1053. [[CrossRef](#)]
12. Xu, F.; Niu, J. Flood disasters and countermeasures in the Huaihe River Basin. *J. Xuchang Univ.* **2004**, *23*, 105–109.
13. Bi, B.; Jiao, M.; Li, Z. Meteorological and hydrological characteristics of floods and rainstorms in the Huaihe River Basin in 2003. *J. Nanjing Meteorol. Inst.* **2004**, *27*, 577–586.
14. Jiao, M.; Jin, R.; Qi, D. Meteorological and hydrological characteristics of Huaihe River rainstorm and flood in 2007. *J. Appl. Meteorol.* **2008**, *19*, 257–264.
15. Nashwan, M.S.; Shahid, S. A novel framework for selecting general circulation models based on the spatial patterns of climate. *Int. J. Climatol.* **2020**, *40*, 4422–4443. [[CrossRef](#)]
16. Huang, X.; Li, X. Future prediction of rainstorm and flood disaster risk in southwest China based on CMIP6. *J. Appl. Meteorol.* **2022**, *33*, 231–243.
17. Feng, Y.; He, Z.; Jiao, S.; Liu, W. Prediction of extreme precipitation scenarios in Guizhou Province based on CMIP6 climate model. *Soil Water Conserv. Res.* **2023**, *30*, 282–290.
18. Jin, N.; Guo, L. The Impact of Extreme Temperatures on Grain Production in the Huaihe River Basin. *Acad. J. Manag. Soc. Sci.* **2023**, *3*, 64–69. [[CrossRef](#)]
19. Guo, R.; Chen, X.; Cai, A. The quantitative effects of climate change and human activity on the vegetation growth in the Yangtze River Basin. *Front. Earth Sci.* **2023**, *11*, 1168384. [[CrossRef](#)]
20. Dewan, A.M.; Corner, R.; Hashizume, M.; Ongee, E.T. Typhoid fever and its association with environmental factors in the Dhaka metropolitan area of Bangladesh: A spatial and time-series approach. *PLoS Neglected Trop. Dis.* **2013**, *7*, e1998. [[CrossRef](#)]
21. Minh, P.T.; Tuyet, B.T.; Thao, T.T.T. Application of ensemble Kalman filter in WRF model to forecast rainfall on monsoon onset period in South Vietnam. *Vietnam J. Earth Sci.* **2018**, *40*, 367–394. [[CrossRef](#)]
22. Zhang, Q.; Li, J.; Singh, V.P.; Xu, C.Y. Copula-based spatio-temporal patterns of precipitation extremes in China. *Int. J. Climatol.* **2013**, *33*, 1140–1152. [[CrossRef](#)]
23. Field, C.B. (Ed.) *Managing the Risks of Extreme Events and Disasters to Advance Climate Change Adaptation: Special Report of the Intergovernmental Panel on Climate Change*; Cambridge University Press: Cambridge, UK, 2012.
24. Ma, J.; Gao, Y. Analysis of annual average and extreme precipitation changes in the upper reaches of the Yellow River in the past 50 years. *Plateau Meteorol.* **2019**, 124–135.
25. Jin, R.; Yang, Y. Evaluation of the CMIP5 global climate model for the simulation of the northward extension of rain belts in eastern China. *Meteorol. Hydro-Ocean. Instrum.* **2022**, *39*, 19–23.
26. Wang, Q.; Zhang, M.; Wang, S.; Luo, S.; Wang, B.; Zhu, X. Analysis of extreme temperature events in the Yangtze River Basin from 1962 to 2011. *Acta Geogr. Sin.* **2013**, *68*, 611–625.
27. Taylor, K.E. Summarizing multiple aspects of model performance in a single diagram. *J. Geophys. Res. Atmos.* **2001**, *106*, 7183–7192. [[CrossRef](#)]
28. Liu, X.; Hu, B.; Ren, Z. Temporal and spatial changes and driving factors of water use efficiency of vegetation ecosystems on the Loess Plateau. *Chin. Agric. Sci.* **2018**, *51*, 302–314. [[CrossRef](#)]
29. Li, S.; Yang, S.; Liu, X. Spatiotemporal variation characteristics and influencing factors of extreme precipitation in the north and south of Qinling-Huaihe River from 1960 to 2013. *Adv. Geogr. Sci.* **2015**, 354–363.
30. Wang, D.; Liu, J.; Wang, H.; Shao, W.; Mei, C.; Ding, X. Performance evaluations of CMIP6 and CMIP5 models for precipitation simulation over the Hanjiang River Basin, China. *J. Water Clim. Chang.* **2022**, *13*, 2089–2106. [[CrossRef](#)]
31. Ngoma, H.; Wen, W.; Ayugi, B.; Babaousmail, H.; Karim, R.; Ongoma, V. Evaluation of precipitation simulations in CMIP6 models over Uganda. *Int. J. Climatol.* **2021**, *41*, 4743–4768. [[CrossRef](#)]
32. Pan, H.; Jin, Y.; Zhu, X. Comparison of projections of precipitation over Yangtze River Basin of China by different climate models. *Water* **2022**, *14*, 1888. [[CrossRef](#)]
33. Pomee, M.S.; Hertig, E. Precipitation projections over the Indus River Basin of Pakistan for the 21st century using a statistical downscaling framework. *Int. J. Climatol.* **2022**, *42*, 289–314. [[CrossRef](#)]

Disclaimer/Publisher’s Note: The statements, opinions and data contained in all publications are solely those of the individual author(s) and contributor(s) and not of MDPI and/or the editor(s). MDPI and/or the editor(s) disclaim responsibility for any injury to people or property resulting from any ideas, methods, instructions or products referred to in the content.